Computational Fluid Dynamics: Analysis of a Real Nasal Airway

48

M. Kürşat Gökcan, S. Nafuna Wanyonyi, and Dilek Funda Kurtuluş

48.1 Introduction

The development and use of personalized medicine have an increasing importance in patient care. Numerical simulations of various biological phenomena have and continue to enable doctors and medical specialists to diagnose patients and understand how practical and effective treatment can be. The paths to patient-specific diagnosis and preoperative planning are slowly being paved and with immense success. Proof of this lies in the major developments made in medical software that have enabled accurate three-dimensional (3D) models of the human organs to be generated for use in analysis, ensuring accurate results. Also, advancements in technology have enabled simulation of surgeries where professionals can make cuts, test out different implant sizes and do much more to the models of organs. This helps the medical practitioner find out the effects of the procedure beforehand by performing analysis of the modified model.

Breathing is a dynamic process between inhaled air, mucosal surfaces and the alveoli. Within the nasal cavity, there are changes of airflow and pressure occurring during the respiratory cycle, as well as exchanges of heat and humidity, and important immune responses to inhaled antigens and allergens [1]. However, evaluation of nasal function with anterior rhinoscopy, nasal endoscopy and/or paranasal CT scan is usually insufficient to make proper assessment of airflow, air-surface interaction and olfaction. There are currently two clinical measurement tools to evaluate airflow parameters: Rhinomanometry measures pressure and airflow during respiration to define the resistance of the nasal airway. Acoustic rhinometry uses the sound

M. K. Gökcan (✉)
Otorhinolaryngology, Head and Neck Surgery Department, Ankara University Medical School, Ankara, Turkey
e-mail: Kursat.Gokcan@medicine.ankara.edu.tr

S. N. Wanyonyi · D. F. Kurtuluş
Department of Aerospace Engineering, Middle East Technical University, Ankara, Turkey
e-mail: kurtulus@metu.edu.tr

C. Cingi et al. (eds.), *Challenges in Rhinology*,
https://doi.org/10.1007/978-3-030-50899-9_48

waves reflected from the nasal walls to create a two-dimensional image of the nasal cavity. These tests have significant limitations since they do not show the entire nasal function, such as local flow and pressure changes, turbulence and heat exchanges [1, 2]. As nasal cavity has a complex geometry which hinders placement of pressure, temperature and humidity sensors throughout the flow, we need a non-invasive and objective method to measure or calculate those parameters.

The utilization of computational fluid dynamics (CFD) for airflow studies has opened a new era. The noninvasive nature of CFD modelling permits us to explore a broad variety of flow simulations, consequently allowing us to monitor pressure and stress variables. More recently, numerical simulations have been increasingly applied to study flow patterns in airways with anatomic abnormalities. By using CFD modelling, quantitative and qualitative information can be obtained on various parameters of airflow, such as flow velocity, static airway wall pressure and pressure drop, turbulence and wall shear stress [3, 4]. The first anatomically accurate 3D computer-generated model of airflow in the nose based on CT scan results was described in 1995 [5]. Since this time CFD modelling has been used to study airflow, heat and humidity exchanges, as well as topical delivery of drugs into the nasal cavity and paranasal sinuses under normal or pathological conditions [1].

In this chapter, the focus is placed on personalized nasal surgery and how the procedure has been enhanced with numerical simulations of respiration. We will venture into details of normal physiologic respiration through the nose and how numerical simulations help as a predictive tool.

48.2 Methodology

48.2.1 Construction of Airway Model

A three-dimensional (3D) anatomically precise patient-specific model is reconstructed from multidetector-computed tomography (MDCT) images of an anonymous maxillofacial scan, from the PACS archive. Volumetric DICOM images with 0.1 mm intervals were carried to commercial medical imaging software, MIMICS® (Materialise, Belgium). The model generated includes the nasal cavity, paranasal sinuses and the nasopharynx. The process begins as CT scans of the subject are loaded into MIMICS and the nasal cavity and airway are identified in each of the axial images based on a predefined thresholding relative to the surrounding tissue. 3D raw models are reconstructed from these masks by surface triangulation and then exported into 3-matic, another Materialise software module. Different views of 3D model obtained are shown in Fig. 48.1.

In 3-matic, the model's boundary conditions are defined and demarcated as individual faces. An inlet, outlet and wall from the 3D surface model are specified by creating a datum plane. Separate datum planes are used for each surface, so that separate boundary surfaces are defined. The datum planes are then appropriately positioned against the 3D model to mark where the boundary surfaces will be created. By using the cut function, under the 'Design' tab, the model nasal cavity is

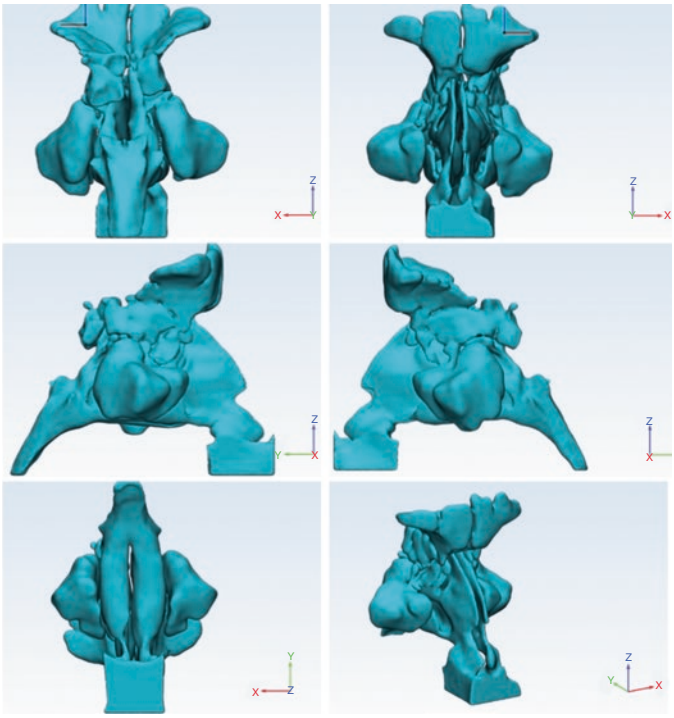

Fig. 48.1 3D model of the nasal cavity, paranasal sinuses and nasopharynx (different views)

then cut into separate parts. The parts that are not needed are then deleted and new surfaces created as a result (Fig. 48.2).

Using the 3-matic software, the surface mesh quality can be improved by smoothing and remeshing, to control the maximum cell edge length and the grid density. Remeshing should be performed after the boundary surfaces are defined, to avoid any changes in the new mesh. The surface mesh should be generated first. The 'Remesh' tab has a variety of options for the type of surface mesh that can be developed. Depending on the grid size and the complexity of the model, a specific type or a combination of mesh types should be chosen. In the current study, an adaptive mesh was generated. The volume mesh was then created.

48.2.2 CFD Modelling

The generated mesh is imported into ANSYS Fluent® (Canonsburg, PA, USA) for analysis to be performed. ANSYS Fluent implements the finite-volume method to solve conservation equations. The pressure-velocity coupling is done by means of the SIMPLE-type fully implicit algorithm. Pressure-velocity coupling is used with a predictor-corrector pressure scheme. The solution is second-order accurate in

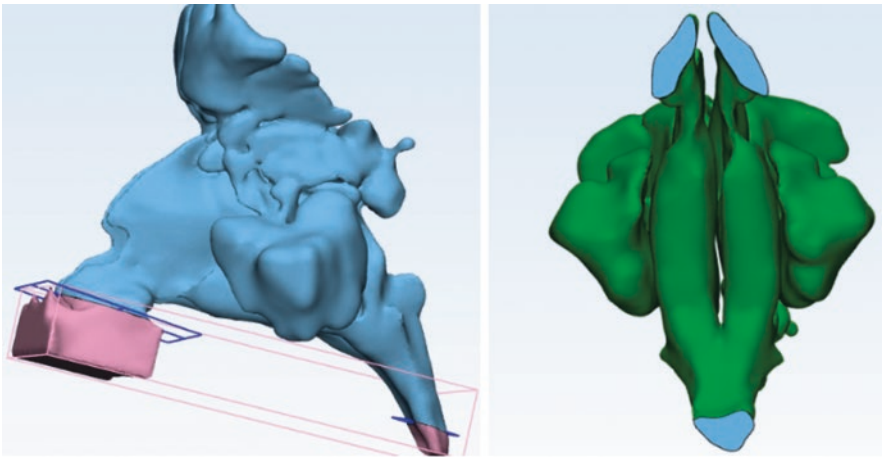

Fig. 48.2 Defining boundary surfaces in 3-matic® (Materialise, Belgium) software

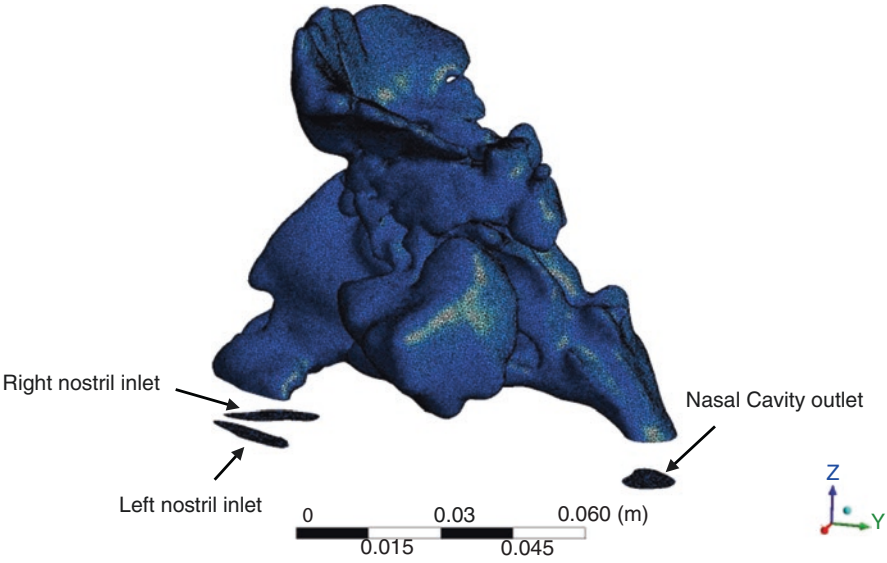

Fig. 48.3 Mesh generated in 3-matic® (Materialise, Belgium) software

space. For the current case study, 3D steady Navier-Stokes equation with the $k - \omega$ turbulence model is used to solve the airway. The mesh comprised of 483,663 cells, 1,072,202 faces and 132,773 nodes (Fig. 48.3).

For boundary conditions, the nose inlets are defined as pressure inlets and assigned 0 Pa as gauge pressure (standard atmospheric pressure). No slip boundary conditions are defined for the inner wall, while the nasal cavity outlet/nasopharynx

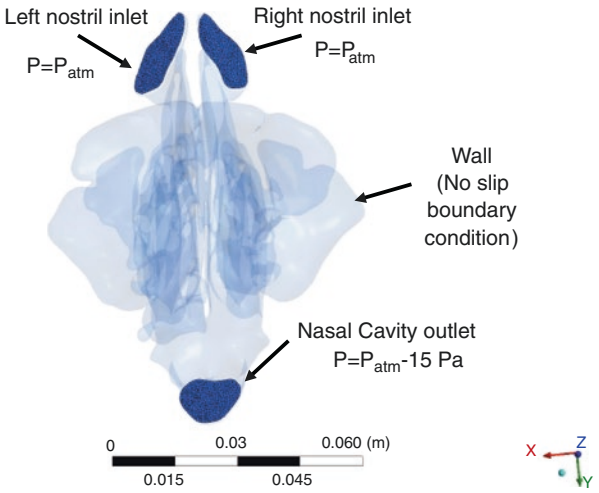

Fig. 48.4 Boundary conditions

is set as a pressure outlet and assigned with −15 Pa as gauge pressure. Figure 48.4 shows the boundary conditions at the nose inlets (nostrils) and the nasal cavity outlet. Atmospheric pressure is taken to be P_{atm} = 101,325 Pa.

48.3 Results

48.3.1 Geometric Representation for Post-processing

The geometry of the nasal airway is very complex. For this purpose, the post processing is performed at specified planes in different plane sections. The model is investigated along the CORONAL, AXIAL and SAGITTAL planes. All the investigated plane sections are shown in Fig. 48.5, while the 2D plane sections corresponding to CORONAL, AXIAL and SAGITTAL planes are shown in Fig. 48.6a–c, respectively. The areas of the various plane sections are tabulated, and the values are shown in Table 48.1. As for the boundary surfaces, the areas are shown in Table 48.2. Note that the right and the left nose inlets have slightly different areas (see also Fig. 48.4). This is important to note because this will be elicited by the resulting velocity and pressure contours drawn at the nostril planes.

48.3.2 Streamlines

Streamlines are drawn to illustrate the flow of air within the nasal cavity (Fig. 48.7). The three-dimensional streamlines indicate that the main flow path is through the inferior meatus. Around the nasal valve and the nasopharynx, the flow is faster than

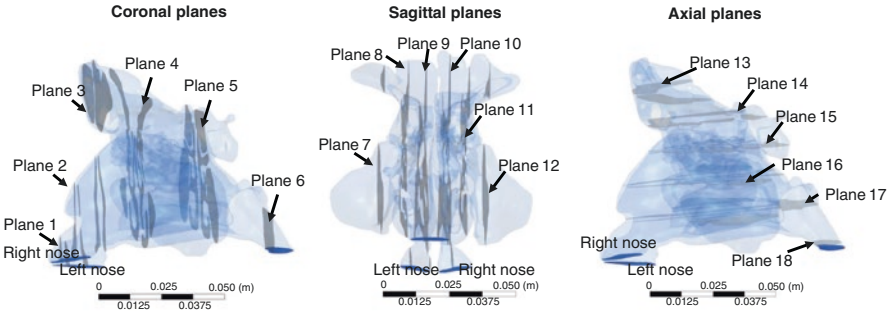

Fig. 48.5 3D model investigated at different plane cuts

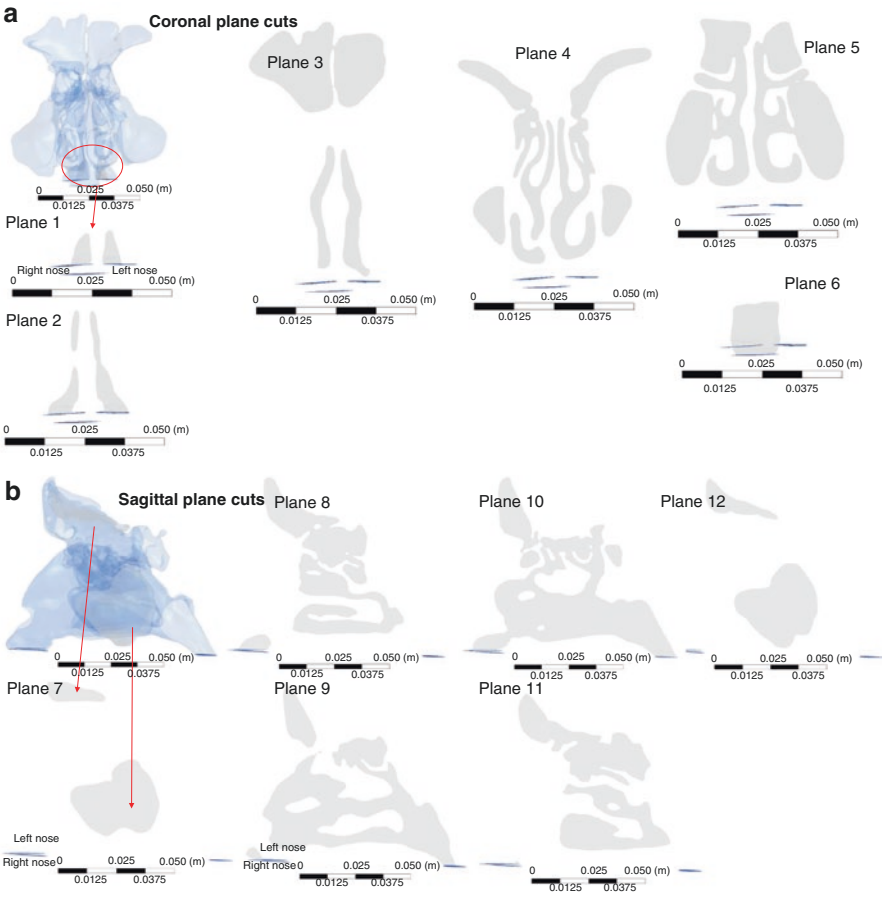

Fig. 48.6 (**a**) Coronal plane cuts. (**b**) Sagittal plane cuts. (**c**) Axial plane cuts

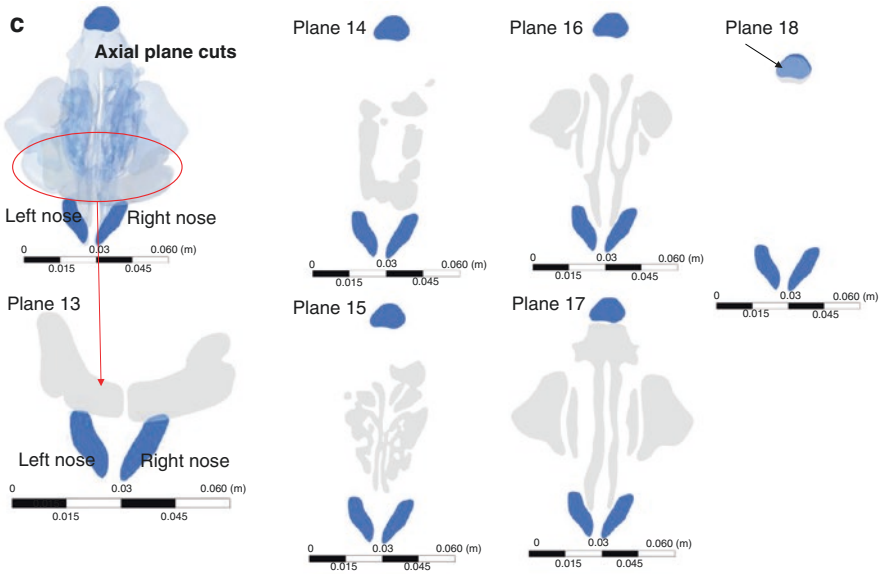

Fig. 48.6 (continued)

Table 48.1 Various plane section areas

Planes	Area (m^2)					
Planes 1–6	0.000088	0.000203	0.00106	0.00117	0.00165	0.000232
Planes 7–12	0.000996	0.00171	0.00239	0.00262	0.00169	0.00110
Planes 13–18	0.000778	0.000682	0.000855	0.00114	0.00198	0.00013

Table 48.2 Boundary surfaces areas

Boundary surface	Right nose inlet	Left nose inlet	Nasal cavity outlet
Area (m^2)	0.0001093	0.0001113	0.0001162

the turbinate section area. The region with the highest velocity is spotted near the choana, the nasopharynx region, where the streamlines elicit this behaviour. There are also sections where vortices are experienced, on the top and bottom sections of the nasal valve and middle turbinate. The formation of the vortices creates at the same time very low suction pressure regions and also increase in the wall shear stresses.

Left and right frontal vortices are generated just after the left and right noses, respectively (Fig. 48.7a, b). The flow initially accelerates in front of these vortices, and then two dominant vortex structures with low pressure cores are visualized in front region of the airway. The streamlines also show a high velocity region before the nasal cavity outlet (Fig. 48.7a). Figure 48.7b also represents the vortex structures formed at both maxillary and frontal sinuses.

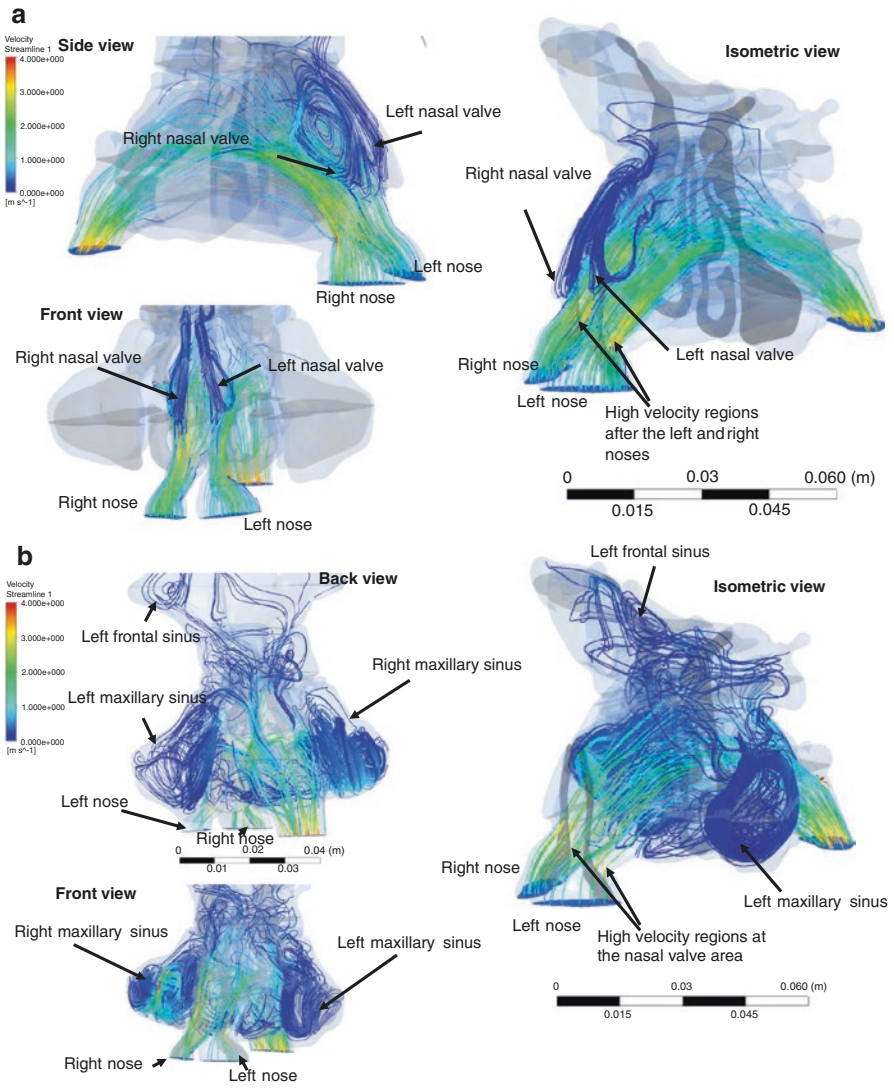

Fig. 48.7 (**a**) Streamlines showing the front vortices. (**b**) Streamlines showing the paranasal sinus ventilation during inspiration

48.3.3 Velocity and Pressure Contours

Velocity magnitude contours for the CORONAL plane cuts are plotted in Fig. 48.8. The contours are drawn at their local contour values to be able to visualize high velocity regions and local pressure drops at each section. The range for the pressure stays within the limits defined as boundary conditions. As expected, the gauge

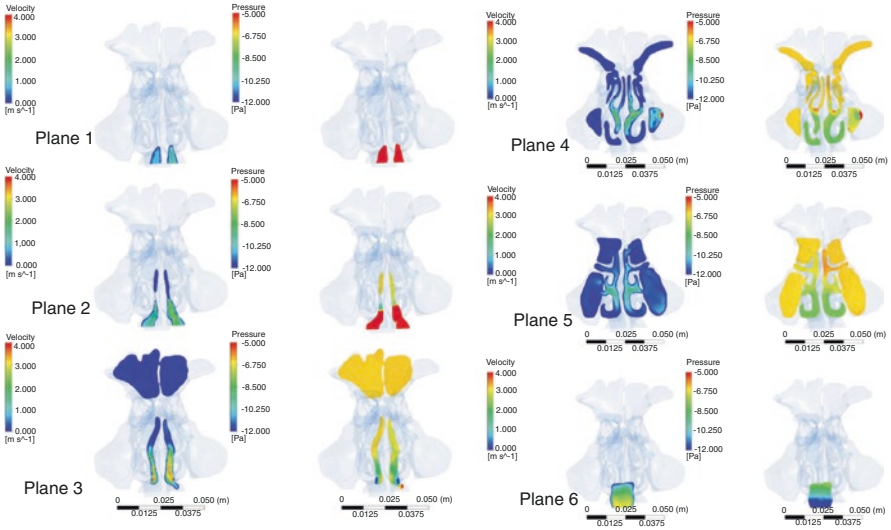

Fig. 48.8 Velocity magnitude (left) and gauge pressure contours (right) in coronal planes

Table 48.3 Average and maximum velocities at the planes

Planes	Average velocities (m/s)					
Planes 1–6	0.971	1.28	0.602	0.346	0.336	1.93
Planes 7–12	2.58×10^{-2}	0.338	0.942	0.790	0.266	0.0608
Planes 13–18	0.00678	0.0772	0.165	0.587	0.609	2.85
Planes	Maximum velocities (m/s)					
Planes 1–6	1.83	7.13	4.68	9.41	2.83	3.42
Planes 7–12	0.382	4.23	3.70	**12.8**	2.03	0.537
Planes 13–18	0.0530	0.470	1.37	5.84	3.55	3.60

pressure gradually decreases from 0 (atmospheric pressure) to −15 Pa as the sections get closer to the nasal cavity outlet.

The average and maximum velocities of each plane along CORONAL, SAGITTAL and AXIAL are also shown in Table 48.3. Along the CORONAL plane, through planes 1 to 6, the average velocity is observed to increase gradually from 0.971 m/s to 1.28 m/s and then decrease while until a high velocity of 1.93 m/s is reached close to the nasal cavity outlet. Along this cut a maximum velocity is observed at plane 4 with 9.41 m/s.

When observing the cuts along SAGITTAL plane, it is observed that the velocities reach maximum value of 12.8 m/s on plane 10 (see Figs. 48.9, 48.10 and 48.11).

Average pressure values on the planes were computed and tabulated in Table 48.4. The pressure values obtained reflect the data stated earlier. The sections closest to the nasopharynx show the lowest values of pressure achieved, for instance, plane 6

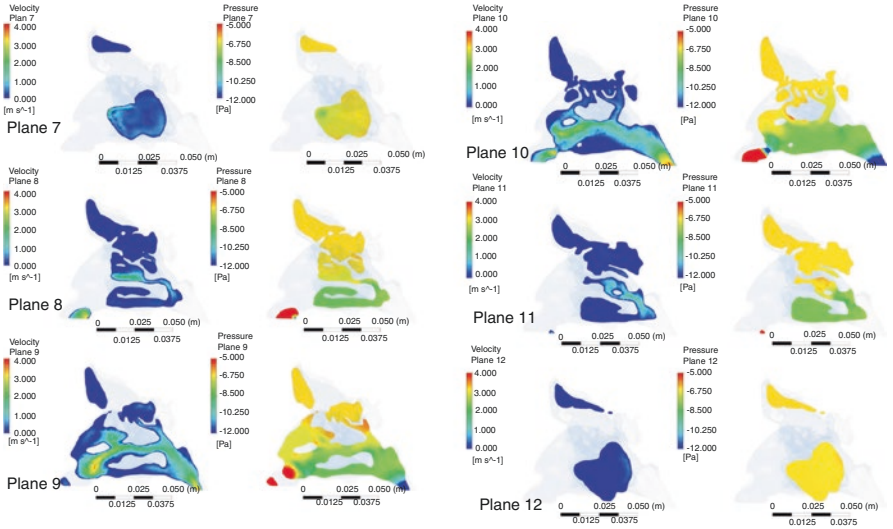

Fig. 48.9 Velocity magnitude (left) and gauge pressure (right) contours in sagittal planes

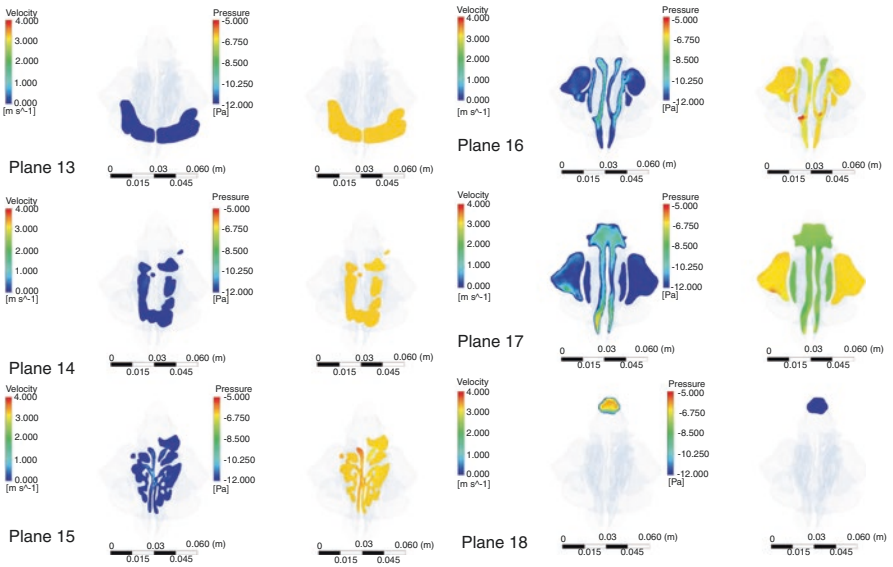

Fig. 48.10 Velocity magnitude (left) and gauge pressure (right) contours in axial planes

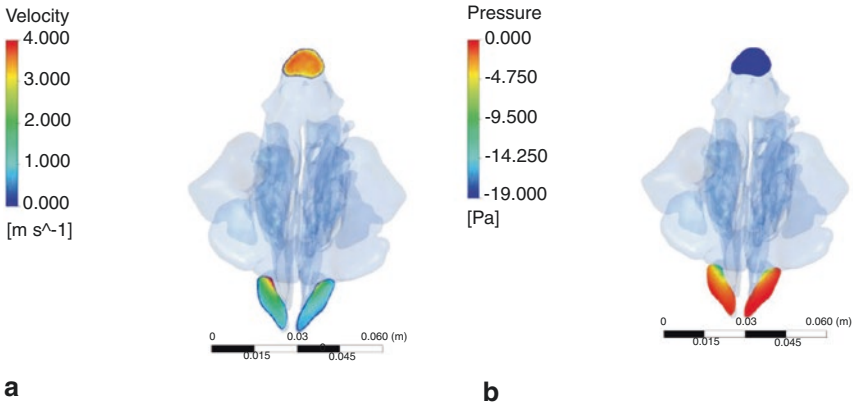

Fig. 48.11 Velocity magnitudes (**a**) and gauge pressure (**b**) contours for boundaries

Table 48.4 Average gauge pressure values at the planes

Planes	Average gauge pressure (Pa)					
Planes 1–6	−0.993	−4.61	−6.69	−6.71	−6.72	−10.4
Planes 7–12	−6.31	−6.79	−6.97	−7.11	−6.98	−6.38
Planes 13–18	−6.32	−6.33	−6.31	−6.56	−7.37	−13.4

Table 48.5 Average velocity values at the boundaries

Boundary surface	Right nostril	Left nostril	Nasal cavity outlet
Velocity (m/s)	1.755	1.183	3.388

Table 48.6 Average gauge pressure values at the boundaries

Boundary surface	Right nostril	Left nostril	Nasal cavity outlet
Pressure (Pa)	−1.067	−2.263	−15.0

registers a value of −8.212 Pa which is the lowest average, closest to −15 Pa. In contrast, plane 1 registers the highest value of pressure with −1.082 Pa as the value. This is in accordance with expectations. The average values of the velocity at the nose inlets and nasal cavity outlet are computed and shown in Table 48.5. The average values of the pressure on all the boundary surfaces are computed and shown in Table 48.6.

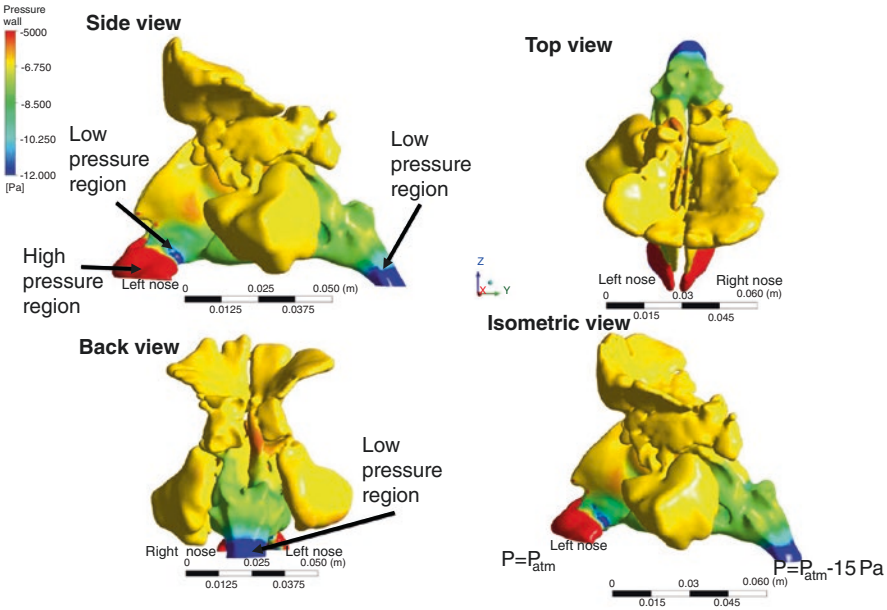

Fig. 48.12 Gauge pressure distribution of the wall

48.3.4 Wall Pressure and Shear Stress Values

For the wall, only shear and pressure contour are plotted. The gauge pressure on the nasal wall is shown in Fig. 48.12. The pressure at the nose inlets is close to atmospheric pressure, and positive pressure values are also observed in the nose regions. The outlet section has −15 Pa gauge pressure as it is given in the boundary conditions. A low-pressure region is also observed just after the nose region.

For wall shear stress is plotted in Fig. 48.13, and the highest wall shear stresses are observed just after the nose inlets and also at the outlet region where the pressure is lowest.

48.4 Discussion and Literature Review

The nose is a dynamic filter that provides humidification, thermoregulation and filtration of the inhaled air, as well as the olfaction function and important immune responses to inhaled antigens. Therefore, complex anatomy with vascular and neural supply of the nose is crucial for executing such a complex function, and of course, there are several things that can go wrong in this complex and delicately balanced system.

Evaluation of nasal patency requires thorough examination with anterior rhinoscopy, nasal endoscopy and paranasal sinus CT that is usually asked to evaluate

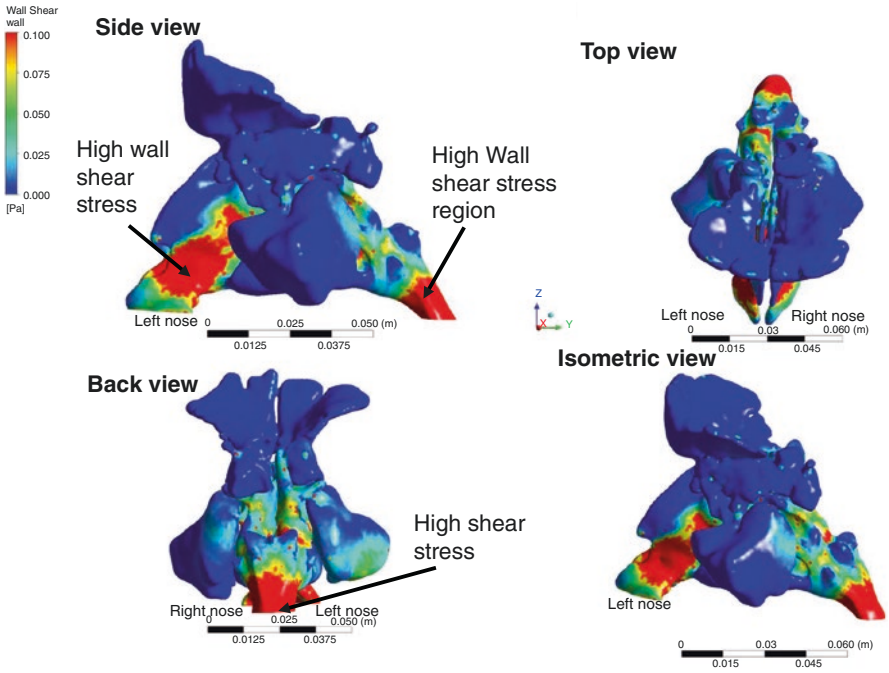

Fig. 48.13 Wall shear stress on the wall

paranasal sinus ostia. Acoustic rhinometry and rhinomanometry can measure cross-sectional areas in nasal cavity and define changes in overall nasal resistance and flow. However, these studies are not able to show sufficient details of dynamic airflow due to the structural complexity of human nose and nasal pathologies. These details can partly be determined by CFD, which enables modelling airflow and air-mucosa interaction by numerical solution of fluid dynamics equations.

Accurate 3D models of the nasal cavity and upper airway have already been seen in literature. For a study performed to investigate how airway geometry affects internal pressure in the upper airway of patients with obstructive sleep apnoea syndrome, an accurate model of the airway is investigated with the region of concern, from the nasopharynx to the hypopharynx by Xu et al. [6]. In another study, to validate the use of computational fluid dynamics (CFD) for human upper airway flow simulations, a precise model of the nasal cavity and the upper airway is provided and used for analysis [7]. Analysis was performed on a 3D sinonasal model of a healthy adult and CFD simulations performed to assess pressure, velocity, wall shear stress and particle resident time. The obtained values helped in better understanding the biological phenomena surrounding the sinuses during respiration [8].

To investigate nasal physiological processes like inspiration, expiration and sniffing, a study was performed on an anatomically exact 3D model of the nasal

and pharyngeal cavity of a healthy adult. Unsteady Navier-Stokes equations were solved and velocity and streamline distribution of airflow visualized. The results distinguished the differences between the types of flow and the olfactory areas they pass through [9]. In another study, airflow dynamics during coughing are investigated. Computer tomography (CT) scans of a patient coughing are obtained and a 3D model of the upper airway and main bronchi generated. From the results, it is determined that there is a linear relation between the maximum velocity, pressure and wall shear stress with the cough peak flow rate [10]. Even the deposition of particles has been evaluated, an important aspect in inhaler drug therapy used to determine where particles that are inhaled will be deposited/settle. The particle deposition for light, normal and heavy breathing is investigated and presented [11]. These and more studies have all been simulated to mimic reality, depict various processes and procedures and help predict what should be done.

Various works focused on personalized nasal surgery and virtual surgery and how CFD simulations aid in preoperative planning have been published. Some works also investigate how efficient a procedure is by performing analysis on CT scans obtained from patients who had undergone the procedure. For one case numerical simulation was performed on the middle turbinate section of the nasal vault of both preoperative and postoperative 3D models generated from CT scans of a patient to investigate the effect on nasal airflow dynamics if a resection is performed. Analysis was carried out for quasi-steady laminar nasal airflow at resting breathing conditions. Focusing on velocity, streamlines, shear stress and pressure drop, it was concluded that for the patient in question, the middle turbinate resection did not affect the overall nasal airflow. Therefore, it was pointed out that CFD analysis can be used as a planning tool to guide the optimization of airflow [12]. It is highlighted that CFD would provide a safe, cost-effective and patient-centred tool in virtual surgery and preoperative planning [13].

Therefore, simulations provide a doorway to reliable patient-specific diagnosis and treatment. Note that studies have been performed to validate the use of CFD to simulate upper airway flows. Also, in an earlier mentioned study, to validate the use of CFD in human upper airway flow simulations, the results obtained from analysis are compared to those obtained from experiments done on a model built from stereolithography. Pressure and velocity values are measured, and the simulation and experiment are carried out with the same conditions. Several numerical approaches are used in CFD during analysis and the authors note that there is good agreement with the results. Eventually, the use of CFD to simulate flow is validated [7]. This is also illustrated when steady-state analysis was performed for inspiratory flow on the entire nasal cavity with normal resting breathing rates taken as boundary conditions at the inlet and outlet of the model. Note that analysis was performed on a virtual post-surgery model and another model generated directly from the CT scans of the same patient having undergone surgery. It was concluded that even with the limitations presented by using CFD to predict such, results from both models showed reasonable correlation [14]. Using this numerical approach, medical practitioners

can develop effective surgery protocol and design drug delivery devices, while gaining deeper insight into physical and biological phenomena.

As our results also indicated, normal nasal flow shows over 50% total pressure drop near the inferior turbinate head and wall shear stress, and the vorticity were lower in the turbinate than in the nasal valve region [12]. However, major flow streamlines and velocity distributions in coronal sections may vary among individuals. Surprisingly, on average, more flow passed through the middle than the inferior meatus and correlated with better patency ratings [15]. The pressure gradients within the sinus cavities varied according to their place of connection to the main passage. Alternations in pressure gradients induced a slight pumping phenomenon close to the ostia, but no movement of air was observed within the sinus cavities [8].

Nasal septum deviation (NSD) is the most common aetiology for nasal airway obstruction (NAO), and septoplasty is a very common surgical procedure. Septal deviations are commonly observed during physical examinations, and surgeons face the challenging question of determining if NSD causes NAO in a given patient or not. In addition to NSD, one may encounter inferior turbinate hypertrophy and/or nasal valve insufficiency in the patient; thus, septoplasty is often recommended with turbinate and/or nasal valve surgery. Quantitative criteria are rarely adopted to select patients for surgery, which may explain why up to 50% of patients report persistent or recurrent symptoms of nasal obstruction postoperatively [16]. Personalized nasal surgery with numerical simulation of respiration enabled otorhinolaryngologists to understand, estimate and define the possible role of the procedure for an individual with NAO.

We would also like to outline some of the limitations that CFD presents in this field. CFD is a time-consuming process, taking several hours of work for preparation of 3D models and simulation of surgeries on these models. Additionally, technique usually requires a high-performance multi-core computer, expensive software(s) and aeronautical engineering. Second, translating CFD findings into patient care and clinical practice is a hard task. For doing this, several authors either compared healthy and pathological subjects or compared the same patient before and after the surgical procedure. Alternatively, CFD findings can be correlated with laboratory evaluations as acoustic rhinometry and rhinomanometry which is still difficult to perform on larger scale of subjects [17]. However, postoperative CFD requires a CT scan, and postoperative CT scan is not always justified as it exposes patients to additional radiation [17]. Moreover, calculation and implementation times are still long for daily practice, as stated.

48.5 Conclusion

The 3D nasal airway is simulated using computational fluid dynamics. The real CT images are reconstructed using the commercial medical imaging software. The software is used to generate and refine to adapt high curvature regions. The generated mesh is utilized to perform 3D CFD simulations. The velocity, pressure contours

and streamlines are visualized at different cross sections of the 3D nasal airway. We conclude that CFD provides clinically useful, logically consistent and understandable information that would otherwise be unavailable [18].

References

1. Leite SHP, Jain R, Douglas RG. The clinical implications of computerised fluid dynamic modelling in rhinology. Rhinology. 2019;57(1):2–9. https://doi.org/10.4193/Rhin18.035.
2. Andre RF, Vuyk HD, Ahmed A, Graamans K, Nolst Trenite GJ. Correlation between subjective and objective evaluation of the nasal airway. A systematic review of the highest level of evidence. Clin Otolaryngol. 2009;34(6):518–25. https://doi.org/10.1111/j.1749-4486.2009.02042.x.
3. Gokcan MK, Gunaydinoglu E, Kurtulus DF. Effect of glottic geometry on breathing: three-dimensional unsteady numerical simulation of respiration in a case with congenital glottic web. Eur Arch Otorhinolaryngol. 2016;273(10):3219–29. https://doi.org/10.1007/s00405-016-4082-6.
4. Gokcan MK, Kurtulus DF, Ustuner E, Ozyurek E, Kesici GG, Erdem SC, et al. A computational study on the characteristics of airflow in bilateral abductor vocal fold immobility. Laryngoscope. 2010;120(9):1808–18. https://doi.org/10.1002/lary.21003.
5. Keyhani K, Scherer PW, Mozell MM. Numerical simulation of airflow in the human nasal cavity. J Biomech Eng. 1995;117(4):429–41. https://doi.org/10.1115/1.2794204.
6. Xu C, Sin S, McDonough JM, Udupa JK, Guez A, Arens R, et al. Computational fluid dynamics modeling of the upper airway of children with obstructive sleep apnea syndrome in steady flow. J Biomech. 2006;39(11):2043–54. https://doi.org/10.1016/j.jbiomech.2005.06.021.
7. Mylavarapu G, Murugappan S, Mihaescu M, Kalra M, Khosla S, Gutmark E. Validation of computational fluid dynamics methodology used for human upper airway flow simulations. J Biomech. 2009;42(10):1553–9. https://doi.org/10.1016/j.jbiomech.2009.03.035.
8. de Gabory L, Reville N, Baux Y, Boisson N, Bordenave L. Numerical simulation of two consecutive nasal respiratory cycles: toward a better understanding of nasal physiology. Int Forum Allergy Rhinol. 2018;8(6):676–85. https://doi.org/10.1002/alr.22086.
9. Ishikawa S, Nakayama T, Watanabe M, Matsuzawa T. Flow mechanisms in the human olfactory groove: numerical simulation of nasal physiological respiration during inspiration, expiration, and sniffing. Arch Otolaryngol Head Neck Surg. 2009;135(2):156–62. https://doi.org/10.1001/archoto.2008.530.
10. Kou G, Li X, Wang Y, Lin M, Zeng Y, Yang X, et al. CFD simulation of airflow dynamics during cough based on CT-scanned respiratory airway geometries. Symmetry. 2018;10(11):595. https://doi.org/10.3390/sym10110595.
11. Rahimi-Gorji M, Pourmehran O, Gorji-Bandpy M, Gorji TB. CFD simulation of airflow behavior and particle transport and deposition in different breathing conditions through the realistic model of human airways. J Mol Liq. 2015;209:121–33. https://doi.org/10.1016/j.molliq.2015.05.031.
12. Zhao K, Jiang J. What is normal nasal airflow? A computational study of 22 healthy adults. Int Forum Allergy Rhinol. 2014;4(6):435–46. https://doi.org/10.1002/alr.21319.
13. Rhee JS, Cannon DE, Frank DO, Kimbell JS. Role of virtual surgery in preoperative planning: assessing the individual components of functional nasal airway surgery. Arch Facial Plast Surg. 2012;14(5):354–9. https://doi.org/10.1001/archfacial.2012.182.
14. Rhee JS, Pawar SS, Garcia GJ, Kimbell JS. Toward personalized nasal surgery using computational fluid dynamics. Arch Facial Plast Surg. 2011;13(5):305–10. https://doi.org/10.1001/archfacial.2011.18.
15. Zhao K, Malhotra P, Rosen D, Dalton P, Pribitkin EA. Computational fluid dynamics as surgical planning tool: a pilot study on middle turbinate resection. Anat Rec (Hoboken). 2014;297(11):2187–95. https://doi.org/10.1002/ar.23033.

16. Moghaddam MG, Garcia GJM, Frank-Ito DO, Kimbell JS, Rhee JS. Virtual septoplasty: a method to predict surgical outcomes for patients with nasal airway obstruction. Int J Comput Assist Radiol Surg. 2020;15:725–35. https://doi.org/10.1007/s11548-020-02124-z.
17. Radulesco T, Meister L, Bouchet G, Giordano J, Dessi P, Perrier P, et al. Functional relevance of computational fluid dynamics in the field of nasal obstruction: a literature review. Clin Otolaryngol. 2019;44(5):801–9. https://doi.org/10.1111/coa.13396.
18. de Wang Y, Lee HP, Gordon BR. Impacts of fluid dynamics simulation in study of nasal airflow physiology and pathophysiology in realistic human three-dimensional nose models. Clin Exp Otorhinolaryngol. 2012;5(4):181–7. https://doi.org/10.3342/ceo.2012.5.4.181.